The Journal of Immunology

Thymocyte-Specific Truncation of the Deubiquitinating Domain of CYLD Impairs Positive Selection in a NF-κB Essential Modulator-Dependent Manner

Ageliki Tsagaratou, Eirini Trompouki, Sofia Grammenoudi, Dimitris L. Kontoyiannis and George Mosialos

J Immunol 2010; 185:2032-2043; Prepublished online 19 July 2010;
doi: 10.4049/jimmunol.0903919
http://www.jimmunol.org/content/185/4/2032

The Journal of Immunology is published twice each month by
The American Association of Immunologists, Inc.,
1451 Rockville Pike, Suite 650, Rockville, MD 20852

Print ISSN: 0022-1767 Online ISSN: 1550-6606.

Thymocyte-Specific Truncation of the Deubiquitinating Domain of CYLD Impairs Positive Selection in a NF-κB Essential Modulator-Dependent Manner

Ageliki Tsagaratou,*,† Eirini Trompouki,†,1 Sofia Grammenoudi,† Dimitris L. Kontoyiannis,† and George Mosialos*,†

The cylindromatosis tumor suppressor gene (*Cyld*) encodes a deubiquitinating enzyme (CYLD) with immunoregulatory function. In this study, we evaluated the role of *Cyld* in T cell ontogeny by generating a mouse (*Cyld*$^{\Delta 9}$) with a thymocyte-restricted *Cyld* mutation that causes a C-terminal truncation of the protein and reciprocates catalytically inactive human mutations. Mutant mice had dramatically reduced single positive thymocytes and a substantial loss of peripheral T cells. The analyses of polyclonal and TCR-restricted thymocyte populations possessing the mutation revealed a significant block in positive selection and an increased occurrence of apoptosis at the double-positive stage. Interestingly, in the context of MHC class I and II restricted TCR transgenes, lack of functional CYLD caused massive deletion of thymocytes that would have been positively selected, which is consistent with an impairment of positive selection. Biochemical analysis revealed that *Cyld*$^{\Delta 9}$ thymocytes exhibit abnormally elevated basal activity of NF-κB and JNK. Most importantly, inactivation of NF-κB essential modulator fully restored the NF-κB activity of *Cyld*$^{\Delta 9}$ thymocytes to physiologic levels and rescued their developmental and survival defect. This study identifies a fundamental role for functional CYLD in establishing the proper threshold of activation for thymocyte selection by a mechanism dependent on NF-κB essential modulator. ***The Journal of Immunology*****, 2010, 185: 2032–2043.**

Ubiquitination is currently emerging as a dominant regulatory mechanism in cancer and immunity by means of posttranslational modification of intracellular signaling mediators of activation, proliferation, stress, and death. The cylindromatosius tumor suppressor gene (*Cyld*) encodes a 956 aa polypeptide (CYLD) with deubiquitinating activity (1–3). The deubiquitinating domain of CYLD is located in the carboxyl terminal 365 aa and constitutes the most highly conserved region of the protein (2–4). *Cyld* originally emerged as a tumor suppressor gene through the identification of human mutations predisposing to tumors of skin appendages (4). Subsequently, insufficient CYLD functions correlated with a range of tumors including hepatocellular, colon, and lung carcinomas and multiple myelomas (5–9). Interestingly, all the mutations identified to date in human *Cyld* are predicted to cause carboxyl terminal truncations or frameshift alterations of the protein that inactivate its deubiquitinating activity (2, 3). Numerous in vitro and in vivo experimental approaches have established an inhibitory role for CYLD on the basal and TNFR-family–induced activity of the transcription factor NF-κB, which was associated with the ability of CYLD to induce the deubiquitination of TNFR-associated factor 2, TNFR-associated factor 6, NF-κB essential modulator (NEMO), TGFβ-activated kinase 1, B cell CLL-lymphoma 3 and receptor-interacting protein 1 (10–12). Notably, the combination of genetic and biochemical studies associated the deubiquitinating activity of CYLD with its tumor-suppressing and NF-κB–inhibitory properties (2, 3).

Interestingly, the armamentarium of CYLD functions extends beyond cellular transformation and includes immune modulation. For example, impaired CYLD expression is associated with immune diseases like inflammatory bowel disease (13). However, a number of recent studies in different mice bearing obligatory null alleles demonstrated putative, essential, yet contrasting roles for CYLD in the regulation of adaptive and innate immune responses (14–18). A first report aimed to eliminate CYLD functions in the mouse through the germ-line removal of the ATG-containing exon 2 from the murine *Cyld* locus (15). Mutant mice were viable but showed reduced numbers of mature $CD4^+$ and $CD8^+$ single positive (SP) T cells in their thymic and peripheral compartments. The study did not reveal the stage of T cell maturation that failed in the context of the mutation. Instead, the authors proposed that defects in the TCR-induced interaction of the lymphocyte-specific protein tyrosine kinase (Lck) adaptor kinase with the ZAP70 kinase obscured the processes of T cell selection in immature *Cyld*-deficient $CD4^+CD8^+$ double positive (DP) thymocytes. Paradoxically, peripheral *Cyld*-deficient T cells did not share the same defect in TCR signaling, but instead were hyperresponsive to TCR stimulation (14). Subsequent studies revealed that these mutant mice exhibited additional abnormalities in B cell development, peripheral B cell subset composition and a puzzling B cell hyperactivity (17). Thus, and although indicative for the involvement of CYLD in the modulation of lymphocyte development, these studies raised a number of puzzling issues and

*School of Biology, Aristotle University of Thessaloniki, Thessaloniki; and †Institute of Immunology, Biomedical Sciences Research Center Alexander Fleming, Vari, Greece

[1]Current address: Harvard Medical School, Children's Hospital, 1 Blackfan Circle, Boston, MA.

Received for publication December 8, 2009. Accepted for publication June 3, 2010.

This work was supported by the Sixth Research Framework Program of the European Union, Project INCA (LSHC-CT-2005-018704), and a Leukemia and Lymphoma Society Scholarship (to G.M.).

Address correspondence and reprint requests to George Mosialos, School of Biology, Aristotle University of Thessaloniki, 54124, Thessaloniki, Greece. E-mail address: gmosialo@bio.auth.gr

The online version of this article contains supplemental material.

Abbreviations used in this paper: BCLX L/S, B cell lymphoma X L/S; DD, double dull; DN, double negative; DP, double positive; IKK, I-κB kinase; LAT, linker for activation of T cells; Lck, lymphocyte-specific protein tyrosine kinase; NEMO, NF-κB essential modulator; PI, propidium iodide; SP, single positive; *tg*, transgenic.

www.jimmunol.org/cgi/doi/10.4049/jimmunol.0903919

could not definitively conclude on the roles of CYLD in governing these processes. The involvement of CYLD in lymphocyte development was questioned further by another line of mouse mutants in which the expression of CYLD was disrupted by the germ-line removal of exons 2 and 3 of the *Cyld* gene (16). Surprisingly, these mice did not appear to have any defects in the development of mature lymphocytes, although these cells showed enhanced activation of NF-κB and JNK in response to stimulators of innate and adaptive immunity. The apparent discrepancy between the different mutants cannot be resolved easily because of the difference in targeting strategies, but they indicate a potential multicellular effect of CYLD in lymphocyte development in addition to potential redundancies in CYLD functions that cannot be resolved in a *Cyld*-deficient setting.

To circumvent these problems and to address the specific role of CYLD in T cell ontogeny, we generated conditionally targeted mice possessing a T cell-restricted mutation in the *Cyld* locus engineered to encode a functionally impaired C-terminal truncated CYLD protein. Through this mutation, we establish a cell-intrinsic role of *Cyld* in T cell development and demonstrate its involvement in thymocyte selection in a manner that depends on its functional interaction with NEMO.

Materials and Methods

Mice

The generation of mice with loxP-targeted *Cyld* locus has been described previously (19). The transgenic *Lck-Cre* (20) mice were provided by J.D. Marth (University of California, San Diego, CA). The transgenic H-Y TCR mice were provided by Dr. B. Malissen (Centre d'Immunologie de Marseille Luminy, Marseille, France). The BL/6 Tg (TCRaTCRb)425 Cbn/j (OT2) mice were purchased from the Jackson Laboratory (Bar Harbor, ME). All mice were maintained in mixed C57BL/6, 129Ola configuration. The mice were bred and maintained in the animal facilities of the Biomedical Sciences Research Centre Alexander Fleming under specific-pathogen free conditions. Experiments on live animals were approved by the Hellenic Ministry of Rural Development (Directorate of Veterinary Services) and by Biomedical Sciences Research Center Alexander Fleming's Animal Research and Ethics Committee for compliance to Federation of Laboratory Animal Science Associations regulations. Screening of tail DNA for inheritance of the floxed *Cyld* gene was performed by PCR using the following primers: F6: 5′-CGTGAACAGATGTGAAGGC-3′; R6: 5′-CTACCATCCCTGCTAACCAC-3′; F5: 5′-GCAGGCTGTACAGATGGAAC-3′; R1: 5′-CTGCAAATTTCAGGTTGCTGTTG-3′. Inheritance of the *LckCre* transgene was determined by PCR using the following primers: forward, 5′-ATTACCGGTCGATGCAACGAGT-3′; and reverse, 5′-CAGGTATCTCTGACCAGAGTCA-3′. Inheritance of the H-Y TCR transgene was determined by PCR using the following primers: Vb8.2HY: 5′-GGCTGCAGTCACCCAAAGCCCAAG-3′ and 5′-CAGTCAGTCTGGTTCCTGAGCC-3′. Inheritance of the OT2 TCR transgene was determined by PCR using the following primers:

oIMR1825: 5′-GCT GCT GCA CAG ACC TAC T-3′ and
oIMR1826: 5′-CAG CTC ACC TAA CAC GAG GA-3′.

DNA analysis for *Nemo* was performed using the following three primers in one reaction, as described elsewhere (21):

27: 5′-GCC TTG GTG CTC CCT AAC TCT-3′,
40: 5′-TCA CAT CAC ATC GTT ATC CTT-3′, and
61: 5′-ATG AAC AAG CAC CCC TGG AAG-3′.

Abs

Abs against the following molecules coupled to the indicated fluorochromes were purchased from BD Pharmingen (San Diego, CA): CD4-FITC, CD4-PE, CD8-PE, CD3–biotin, B220-Cychrome, TCR-Cychrome, CD11b-PE, Gr1-biotin, CD25-biotin, CD44-FITC, CD62L-biotin, CD69 PECy7, and TCRVβ 5.1-PE. The following purified Abs were purchased from BD Pharmingen: anti-NEMO (C73-764), anti-CD53 (OX-79), and anti-CD4 (GK1.5). Biotin-conjugated anti-CD24, allophycocyanin–Cy7-conjugated anti-CD8, anti-CD3ε, and anti-CD28 were purchased from Biolegend (San Diego, CA). A700-conjugated anti-CD4, PercP-conjugated anti-CD8, FITC-conjugated anti–H-Y TCR (clone T3.70), FITC-conjugated anti-TCRVa2 were purchased from eBioscience (San Diego, CA). Determination of cell survival in fresh or cultured thymocytes was conducted by staining with annexin V (BD Biosciences, San Jose, CA) and propidium iodide ([PI] Sigma-Aldrich, St. Louis, MO) after surface staining for CD4 and CD8 (when evaluating survival of total thymocytes) or after CD53-dependent isolation of DP thymocytes. The anti-CYLD Ab that was used in Fig. 1 was a gift from Dr. Shao Cong Sun (MD Anderson Cancer Center, Houston, TX), and it has been described elsewhere (22). The anti-CYLD Ab (E-4) that was used in Supplemental Fig. 6 was purchased from Santa Cruz Biotechnology (Santa Cruz, CA). The anti-Lck (3A5), anti–ZAP-70 (1E7.2), anti-p65 (A), anti–p-JNK (G-7), anti-JNK2 (D-2), anti-linker for activation of T cells (LAT; M-19), and anti-tubulin (B-7) Abs were obtained from Santa Cruz Biotechnology. Abs to Src phosphorylated at tyrosine 416 (which recognizes Lck phosphorylated at tyrosine 394), Zap70 phosphorylated at tyrosine 319, and LAT phosphorylated at tyrosine 191 were obtained from Cell Signaling Technology (Beverly, MA). The anti-actin mouse mAb was purchased from MP Biomedicals (Solon, OH) and the anti-FLAG (M5) mouse mAb was purchased from Sigma-Aldrich.

Flow cytometric analysis

Single-cell suspensions were obtained from the thymus, spleen, and lymph nodes by dissociation of isolated tissues through a 60-μm mesh. Red blood cells were excluded by Gey's lysis solution, and debris was removed by a cell strainer. Cells were processed for the detection of a panel of cell markers by incubation in PBS, 0.1% NaN_2, and 2% FBS for 20 min on ice by titrated concentrations of reagents. Cell-associated fluorescence was analyzed by a FACSCantoII flow cytometer and the DIVA V6 software (BD Biosciences). Flow cytometry figures were prepared using the FlowJo software (Tree Star, Ashland, OR). Differences in lymphocyte populations were evaluated with the unpaired *t* test using the Sigmaplot 9 statistical software.

DP thymocyte purification

Total thymocytes were incubated with anti–CD53-biotin (BD Pharmingen) and then with anti-rat IgG-biotin (Jackson ImmunoResearch Laboratories, West Grove, PA). $CD53^+$ cells were subsequently removed using anti-biotin microbeads (MACS; Miltenyi Biotec, Auburn, CA). DP thymocytes were incubated on ice before stimulation to evaluate TCR signaling.

Immunoblotting and immunoprecipitation assays

Immunoblotting and immunoprecipitation assays were performed as previously described (2).

EMSA

Nuclear extracts were prepared and EMSA was performed as previously described (19). The sequences of the oligonucleotides that were used for the determination of Oct-1 binding were the following:

Oct-1 F: 5′-TGT CGA ATG CAA ATC ACT AG-3′ and
Oct-1 R: 5′-TTC TAG TGA TTT GCA TTC G-3′.

The sequences of the oligonucleotides that were used for the determination of NF-κB binding contained two tandem repeated NF-κB binding sites (underlined), and they were as follows:

NF-κBf: 5′-ATC AGG GAC TTT CCG CTG GGG ACT TT-3′ and
NF-κBr: 5′-CGG AAA GTC CCC AGC GGA AAG TCC CT-3′.

For supershift analysis, nuclear extracts were preincubated with anti-p65 Abs.

T cell stimulation assays

To evaluate TCR signaling, 5×10^6 to 10×10^6 T cells resuspended in serum-free Iscove's medium were incubated for 15 min on ice with anti-mouse CD3ε mAb (1 μg/ml, 145-2c11; Biolegend) and anti-CD4 (1 μg/ml, L3T4; BD Pharmingen), followed by crosslinking with goat anti-hamster IgG (6060-01; SouthernBiotech, Birmingham, AL) for the indicated times at 37°C with gentle shaking. Stimulated T cells were immediately lysed in RIPA buffer containing protease and phosphatase inhibitors. DP thymocyte survival was calculated as the percentage of alive cells (negative for staining with annexin V and PI) after overnight incubation with 20 μg/ml of immobilized anti-mouse CD28 (37.51) and the indicated concentrations of anti-mouse CD3 (145-2c11; Biolegend).

RT-PCR

Total RNA was isolated from total thymocytes or DP cells with Trizol (Invitrogen, Carlsbad, CA) and oligo-dT primed cDNA was prepared using Improm Reverse Transcriptase (Promega, Madison, WI) according to the manufacturer's instructions.

Results

Mutation of Cyld *prohibits the generation of mature thymocytes*

To examine the functional role of *Cyld* in specific tissues, we devised a conditional strategy to render murine CYLD catalytically inactive in tissues of interest. Furthermore, this approach was adopted specifically to elucidate the biologic role of the catalytic domain of CYLD. Previous approaches analyzed the phenotype of *Cyld* null mice, which reflects the combined lack of biologic functions that depend on the multiple functional domains of CYLD. Using gene targeting, we previously flanked the ninth exon of the murine *Cyld* gene with loxP sequences ($Cyld^{flx9}$ allele; Fig. 1*A*) to permit its excision by the Cre recombinase ($Cyld^{\Delta 9}$; Fig. 1*A*) (19). Exon 9 encodes an essential part of the deubiquitinating domain of CYLD; therefore, its removal should inhibit its catalytic activity. Furthermore, the removal of exon 9 should also induce a frameshift mutation because of the aberrant splicing of exons 8 to 10, thus mimicking the naturally occurring carboxyl terminal mutations of *Cyld* in patients with familial cylindromatosis. Previously, we used $Cyld^{flx9/flx9}$ to introduce the $Cyld^{\Delta 9}$ mutation in the mouse germline (19).

To generate mice with a thymocyte-specific $Cyld^{\Delta 9}$ mutation, $Cyld^{flx9/flx9}$ mice were crossed to *LckCre*-transgenic mice (20). The *Lck* promoter restricts the expression of Cre in the early stage of immature double negative (DN) thymocytes. In accordance with the thymocyte-specific expression pattern of the Cre recombinase in *LckCre-*$Cyld^{flx9/flx9}$ mice, the excision of *Cyld* exon 9 was readily evident in thymocytes (Fig. 1*B*), but not in other non-lymphoid tissues from these mice (Fig. 1*C*). In addition, RT-PCR analysis verified the presence of *Cyld* mRNA encoding exons 1–13, but were devoid of the sequence encoding exon 9 (Fig. 1*D* and data not shown). Interestingly, the mutant mRNA was primarily present in *LckCre-*$Cyld^{flx9/flx9}$, whereas it was clearly underrepresented in heterozygous *LckCre-*$Cyld^{flx9/+}$, suggesting a predominance of wild type CYLD expression in the latter setting (Fig. 1*D*). Finally, immunoblotting with an anti-CYLD Ab indicated a nearly complete absence of full-length CYLD protein in *LckCre-*$Cyld^{flx9/flx9}$ thymic or peripheral T cell extracts, respectively (Fig. 1*E*, 1*F*). A carboxyl terminally truncated form of CYLD could not be detected in *LckCre-*$Cyld^{flx9/flx9}$ thymocytes, most likely because the highest level of CYLD expression is observed in SP thymocytes (15), which are practically eliminated in *LckCre-*$Cyld^{flx9/flx9}$ mice (see below).

Both thymic and peripheral T cells isolated from $Cyld^{flx9/+}$ and *LckCre* mice maintained a physiologic representation of T cell subtypes, as assessed by their enumeration after the evaluation of surface expression of CD4, CD8, CD25, CD44, CD62L, CD69, CD5, and TCR (Supplemental Fig. 1 and data not shown). Similarly, the *LckCre-*$Cyld^{flx9/+}$ and *LckCre* mice showed similar representation of T cell subtypes based on the expression of the aforementioned markers (Supplemental Fig. 1*B* and data not shown). Thus, we present *LckCre-*$Cyld^{flx9/+}$ mice (termed *T-*$Cyld^{+}$ in all the figures) as the control animals for mutant *LckCre-*$Cyld^{flx9/flx9}$ mice (termed *T-*$Cyld^{\Delta 9}$ in all the figures).

The introduction of $Cyld^{\Delta 9}$ in mouse thymocytes in *LckCre-*$Cyld^{flx9/flx9}$ did not affect significantly the representation of DN and DP thymocytes; strikingly however, both $CD4^{+}$ and $CD8^{+}$ SP compartments were reduced to almost nominal values (Fig. 2*A*, 2*B*, 2*E*, 2*F*). Furthermore, the reduction in CD4- or CD8-expressing thymocytes reflected the loss of mature single positive subsets, as confirmed by the enumeration of $CD24^{lo}$ cells expressing high levels of surface TCRβ (Fig. 2*C*, 2*D*). However, the $TCR\beta^{lo}CD8^{+}CD5^{-}CD24^{hi}$ thymocytes that constitute immature single positive cells were present, and generally the levels of $CD8^{+}TCR\beta^{lo}$ thymocytes in $Cyld^{\Delta 9}$ and control mice were comparable, whereas $CD8^{+}TCR\beta^{hi}$ thymocytes that represent mature CD8 SP were significantly underrepresented in $Cyld^{\Delta 9}$ mice (Fig 2*G*, 2*H*). Similarly, the reduction of $Cyld^{\Delta 9}$ SP thymocyte populations was also reflected in the dramatic reduction of $CD4^{+}$ and $CD8^{+}$ T cells in the periphery of *LckCre-*$Cyld^{flx9/flx9}$, as assessed by their enumeration in mesenteric lymph nodes and the spleen

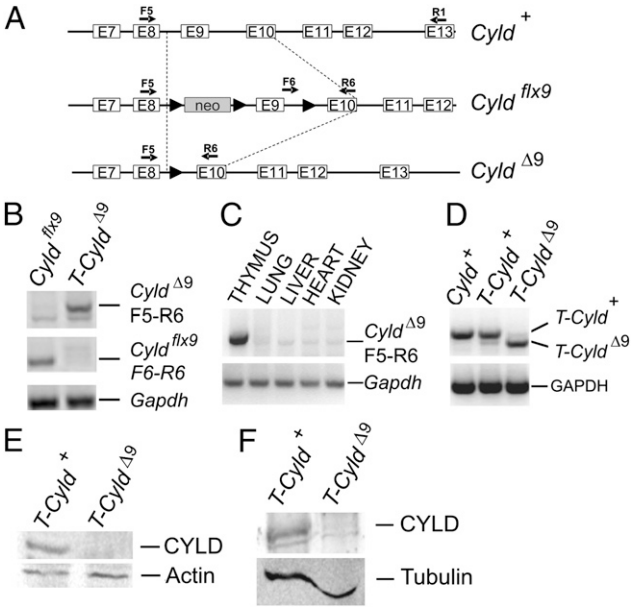

FIGURE 1. Generation and characterization of *LckCre-*$Cyld^{flx9/flx9}$ mice. *A,* Gene-targeting strategy. Schematic representation of exons 7–13 (E7–E13) of the murine *Cyld* locus ($Cyld^{+}$). The structures of the floxed *Cyld* locus in the absence ($Cyld^{flx9}$) and presence ($Cyld^{\Delta 9}$) of the Cre recombinase are shown. The loxP sites are shown as solid triangles, and the neomycin resistance gene is shown as a gray rectangle. The positions of primers F5, F6, R1, and R6 are shown by arrows. *B*, PCR of genomic DNA from thymocytes of $Cyld^{flx9/flx9}$ ($Cyld^{flx9}$) and *LckCre-*$Cyld^{flx9/flx9}$ (*T-*$Cyld^{\Delta 9}$) mice with the indicated primer pairs for the *Cyld* locus or primers for the *Gapdh* locus. The positions of the specific PCR products are indicated. More than four animals per genotype were analyzed. At least three independent experiments were performed. *C*, PCR of genomic DNA from perfused thymus, lung, liver, heart, and kidney of *LckCre-*$Cyld^{flx9/flx9}$ mice with the indicated primer pairs for the *Cyld* locus or primers for the *Gapdh* locus. The positions of the specific PCR products corresponding to the recombined $Cyld^{\Delta 9}$ locus or the *Gapdh* locus are indicated. Organs isolated from two animals were used. Two independent experiments were performed. *D,* RT-PCR of RNA from thymocytes of wild type ($Cyld^{+}$), *LckCre-*$Cyld^{flx9/+}$ (*T-*$Cyld^{+}$) and *LckCre-*$Cyld^{flx9/flx9}$ (*T-*$Cyld^{\Delta 9}$) mice with the primers F5 and R1 for the *Cyld* mRNA or primers for the *Gapdh* mRNA. The position of the specific PCR products corresponding to full-length *Cyld* (*T-*$Cyld^{+}$) and $Cyld^{\Delta 9}$ (*T-*$Cyld^{\Delta 9}$) are indicated. At least three mice per genotype were used. Data are representative of three independent experiments. *E,* Immunoblot of thymocyte lysates from *LckCre* (*T-*$Cyld^{+}$) and *LckCre-*$Cyld^{flx9/flx9}$ (*T-*$Cyld^{\Delta 9}$) mice. The positions of full length CYLD and actin are shown. At least three animals per genotype were used. Data are representative of three independent experiments. *F,* Immunoblot of splenic T cells from *LckCre* (*T-*$Cyld^{+}$) and *LckCre-*$Cyld^{flx9/flx9}$ (*T-*$Cyld^{\Delta 9}$) mice. The positions of full-length CYLD and tubulin are shown. Two animals per genotype were used. Data are representative of two independent experiments.

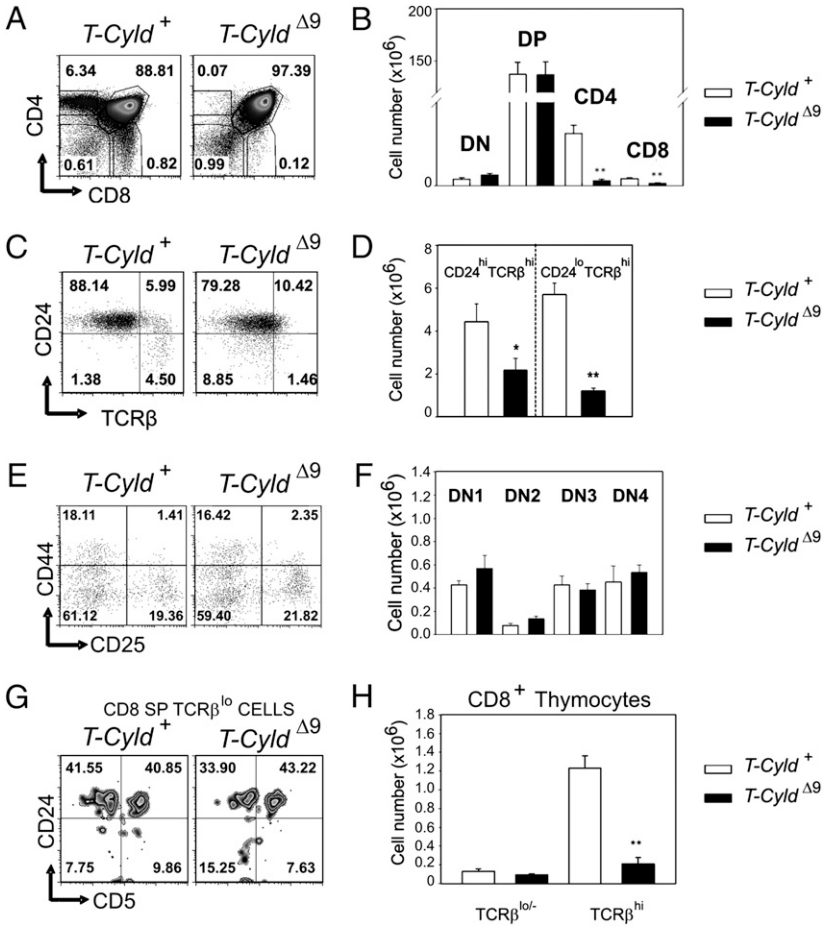

FIGURE 2. Abnormal thymocyte development in *LckCre-Cyld*$^{flx9/flx9}$ mice. *A*, Representative subset distribution of thymocytes derived from control (*LckCre-Cyld*$^{flx9/+}$ [*T-Cyld*$^{+}$]) and mutant (*LckCre-Cyld*$^{flx9/flx9}$ [*T-Cyld*$^{\Delta 9}$]) mice by means of CD4 and CD8 expression. *B,* Enumeration of thymocyte subsets as assessed in *A*. Data are depicted as mean absolute numbers (± SEM) from $n = 6$ mice per group at 6–8 wk of age. $^{**}p = 6.6 \times 10^{-6}$; $^{**}p = 7 \times 10^{-5}$ indicate the statistically significant differences in CD4$^+$ and CD8$^+$ thymocytes between control (*T-Cyld*$^+$) and mutant (*T-Cyld*$^{\Delta 9}$) mice, repectively. *C*, Representative flow cytometric detection of total thymocytes from control (*T-Cyld*$^+$) and mutant (*T-Cyld*$^{\Delta 9}$) mice by means of CD24 and TCRβ expression. *D*, Enumeration of CD24- and TCRβ-defined thymic subsets as assessed in *C*. Data are depicted as mean absolute numbers (± SEM) from $n = 6$ mice per group at 6–8 wk of age. $^{*}p = 0.048$; $^{**}p = 0.00001$ indicate the statistically significant differences in CD24^{hi}TCRβ^{hi} and CD24^{lo}TCRβ^{hi} thymocytes between control (*T-Cyld*$^+$) and mutant (*T-Cyld*$^{\Delta 9}$) mice, respectively. *E*, Representative flow cytometric detection of DN thymocytes from control (*T-Cyld*$^+$) and mutant (*T-Cyld*$^{\Delta 9}$) mice by means of CD25and CD44 expression. Numbers indicate frequency of DN1 (CD44$^+$CD25$^-$), DN2 (CD44$^+$CD25$^+$), DN3 (CD44$^-$CD25$^+$), and DN4 (CD44$^-$CD25$^-$) subsets. *F*, Enumeration of DN1–DN4 subsets as assessed in *E*. Data are depicted as mean absolute numbers (± SEM) from $n = 6$ mice per group at 6–8 wk of age. *G*, Normal immature single positive cell representation, but a dramatically reduced number of mature CD8 SP in *T-Cyld*$^{\Delta 9}$ mice. Representative flow cytometric detection of CD8$^+$TCRβ^{lo} thymocytes from control (*T-Cyld*$^+$) and mutant (*T-Cyld*$^{\Delta 9}$) mice by means of CD5 and CD24 expression in gated CD8$^+$TCRβ^{lo}. *H*, Enumeration of CD8$^+$TCRβ^{lo} thymocytes and mature CD8$^+$TCRβ^{hi} as assessed by means of TCRβ expression in CD8$^+$ gated cells. Data are depicted as mean absolute numbers (± SEM) from $n = 5$ mice per group at 6–8 wk of age. $^{**}p < 0.001$ indicates the statistically significant differences in CD8$^+$TCRβ^{hi} between control (*T-Cyld*$^+$) and mutant (*T-Cyld*$^{\Delta 9}$) mice. In all cases, data are representative of more than two independent experiments.

(Supplemental Fig. 2*A*, 2*B*). Most of the remnant peripheral T cells in *LckCre-Cyld*$^{flx9/flx9}$ possessed CD44^{hi}CD62L^{lo} effector-memory–like phenotype (Supplemental Fig. 2*C*) and a relatively high percentage of them were also CD69$^+$ (Supplemental Fig. 2*D*), suggesting that they are undergoing lymphopenia-induced expansion as described in other lymphopenic states (23, 24).

In contrast, we did not detect any significant difference in the representation of splenic B cells (B220$^+$) and myeloid cells (CD11b$^+$, Ly6G/Gr1$^+$) between controls and *LckCre-Cyld*$^{flx9/flx9}$ mice (data not shown). Collectively, our data demonstrate that the *Cyld*$^{\Delta 9}$ mutation impairs the generation of SP thymocytes in the mouse.

Cyld$^{\Delta 9}$ *thymocytes exhibit late stage selection abnormalities*

The demise of *Cyld*$^{\Delta 9}$ SP thymocytes could be due to defects in their maturation from the corresponding DP pool as a consequence of a block in positive selection. During this process, the phenotype of DP cells changes to reflect a state of activation prior to the acquisition of a single CD4$^+$ or CD8$^+$ coreceptor phenotype. These changes include the increase in surface TCR expression from intermediate (TCRβ^{int}) to high (TCRβ^{hi}) levels, the transient expression of the early activation marker CD69 (25), and the increase in the expression of the TCR-associated molecule CD5 (26) marking the initiation of selection. In wild type mice, TCR$^{-/lo}$CD69$^-$ cells consist of preselection DP thymocytes, TCR^{int}CD69$^{lo/hi}$ are cells initiating and undergoing positive selection, whereas TCR^{hi} CD69^{hi} and TCR^{hi}CD69$^{lo/-}$ represent mainly postselection thymocytes (27). As shown in Fig. 3, *Cyld*$^{\Delta 9}$ DP thymocytes were capable of initiating positive selection, because TCRβ^{int}CD69$^{lo/hi}$ DP thymocytes were more abundant in *LckCre-Cyld*$^{flx9/flx9}$ mice than in control mice (Fig. 3*B*). However, an apparent block at the double dull (DD) developmental stage of *Cyld*$^{\Delta 9}$ DP thymocytes was noted,

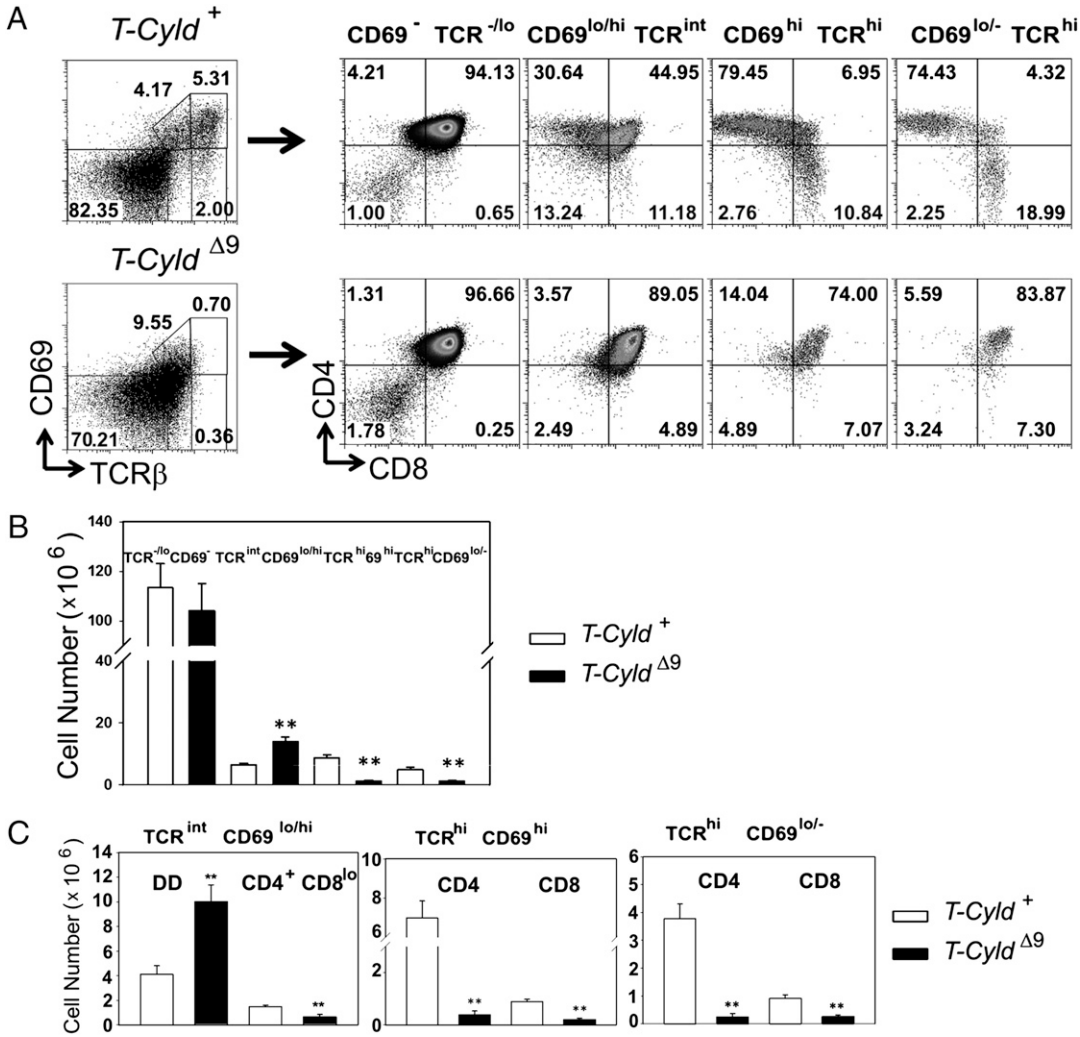

FIGURE 3. *Cyld* $^{\Delta 9}$ DP thymocytes initiate positive selection but are blocked in the double dull developmental stage. *A*, Monitoring of thymocyte positive selection based on CD69 upregulation. Representative flow cytometric detection of CD69 and TCRβ expression in total thymocytes from control (*T-Cyld*$^+$) and mutant (*T-Cyld*$^{\Delta 9}$) mice (*left panels*). Defined subsets representing distinct developmental stages (TCRβ$^{-/lo}$CD69$^-$, TCR^{int}CD69$^{lo/hi}$, TCR^{hi}CD69^{hi}, and TCR^{hi}CD69$^{lo/-}$) were further analyzed for CD4 and CD8 expression (*right panels* indicated by arrows). *B*, Absolute numbers of thymocyte subsets in control (*T-Cyld*$^+$) and mutant (*T-Cyld*$^{\Delta 9}$) mice as assessed by CD69 and TCR expression in *A*. Data are depicted as mean absolute numbers (± SEM) from $n = 6$ mice per group at 5–7 wk of age. $^{**}p < 0.001$ indicates the statistically significant differences in the different developmental stages between control (*T-Cyld*$^+$) and mutant (*T-Cyld*$^{\Delta 9}$) mice. *C*, Enumeration of thymic subsets defined by CD4 and CD8 expression within the CD69/TCR defined developmental stages that showed significant statistical difference in *B*. Data are depicted as mean absolute numbers (± SEM) from $n = 6$ mice per group at 5–7 wk of age. The statistically significant differences between control (*T-Cyld*$^+$) and mutant (*T-Cyld*$^{\Delta 9}$) mice: $^{**}p < 0.02$ for DD cells; $^{**}p < 0.001$ for the other subsets.

because CD4$^+$CD8^{lo} cells were dramatically reduced in *Cyld*$^{\Delta 9}$ mice (Fig. 3*C*). Furthermore, immature TCR^{hi}CD69^{hi} SP thymocytes and mature TCR^{hi}CD69$^{lo/-}$ SP thymocytes were dramatically reduced, whereas remnant cells that express these markers exhibited a latent DD identity and showed similar percentages of CD4 and CD8 SP thymocytes instead of the typical 3:1 ratio of CD4 to CD8 SP thymocytes (Fig. 3*C*). Similar conclusions were reached when evaluating the upregulation of CD5 in combination with TCR. More specifically, the following four different developmental stages of thymocytes can be discerned based on the expression of CD5 and TCR: TCR^{lo}CD5^{lo} cells that consist of preselection DP cells; TCR^{lo}CD5^{int} cells that consist of DP undergoing positive selection; TCR^{int}CD5^{hi} cells that are mainly DD as well as CD4$^+$ CD8^{lo} cells that are in the process of positive selection; and, finally, TCR^{hi}CD5^{hi} cells that consist of postselection CD4 and CD8 thymocytes (27). As shown in Supplemental Fig. 3*A*, *Cyld*$^{\Delta 9}$ DP cells initiated the process of positive selection as indicated by the overrepresentation of TCR^{lo}CD5^{int} cells compared with control thymocytes. However, *Cyld*$^{\Delta 9}$ cells were blocked in the DD developmental stage and failed to upregulate TCR, a hallmark of the successful completion of positive selection and the generation of mature naive SP cells ready to migrate to the periphery (Supplemental Fig. *3A*, 3*B*) (28). As expected, CD4$^+$CD8^{lo} cells were severely reduced and SP cells were practically absent in mutant mice (Supplemental Fig. 3*A*–*C*). Collectively, our data indicate that *Cyld*$^{\Delta 9}$ DP cells initiate the process of positive selection and proceed until the DD stage where they are apparently blocked, resulting in a nearly complete absence of CD4$^+$CD8^{lo} cells and CD5^{hi}CD69$^{lo/-}$ TCR^{hi} mature SPs. This deviation of thymocytes from the normal developmental process could be attributed either to their deletion or to their inability to complete positive selection, potentially because of impaired TCR signaling. However, the normal initiation of positive selection and the presence of cells undergoing positive selection until the DD stage—that is, until the upregulation of TCR (Fig. 3 and Supplemental Fig. 3)—suggests that there is no major defect in TCR signaling in *Cyld*$^{\Delta 9}$ mice (27). Indeed, proximal TCR signaling in response to CD3/CD4 costimulation was similar in *Cyld*$^{\Delta 9}$ and control DP thymocytes (Supplemental Fig. 4*A*). To explore further the

reason for the loss of *Cyld*$^{\Delta 9}$ DP thymocytes, we evaluated their survival rate in ex vivo cultures. As assessed by annexin V and PI staining, more than 70% of control *LckCre-Cyld*$^{flx9/+}$ DP thymocytes survived after a 20-hr ex vivo culturing period. In sharp contrast, less than 30% of *LckCre-Cyld*$^{flx9/flx9}$ DP thymocytes survived under the same conditions (Fig. 4*A*, 4*B*). More precisely, both the early and late apoptotic *Cyld*$^{\Delta 9}$ DP were 2-fold higher when compared with control DP thymocytes, whereas necrotic DP cells could be detected in similar percentages (Fig. 4*A*). Intriguingly, the expression of the prosurvival factor B cell lymphoma X L/S (BCLX$_{L/S}$), which is a critical player in the survival of DP thymocytes (29, 30), was significantly reduced in *Cyld*$^{\Delta 9}$ compared with control DP thymocytes, providing a molecular basis for the impaired survival of *Cyld*$^{\Delta 9}$ DP thymocytes (Fig. 4*C*, 4*D*).

Transgenic TCRs that favor positive selection failed to rescue the development of Cyld$^{\Delta 9}$ *DP thymocytes and revealed their increased propensity for deletion*

The complex process of thymocyte selection is difficult to unravel in mice with a polyclonal T cell repertoire. To circumvent this obstacle, we examined the selection of MHC class I restricted thymocytes expressing the transgenic HY TCR. This transgenic TCR reacts with an Ag derived from the male-specific Smcy protein in the context of H-2D^b MHC class I. Hence, thymocytes expressing HY-specific TCR are negatively selected in male H-2D^b and undergo massive deletion. This phenomenon leads to a dramatic decrease in total cellularity, which is accompanied by severe underrepresentation of DP and CD8 SP T cells. However, HY-specific TCR promotes positive selection of the CD8 lineage in female mice (31).

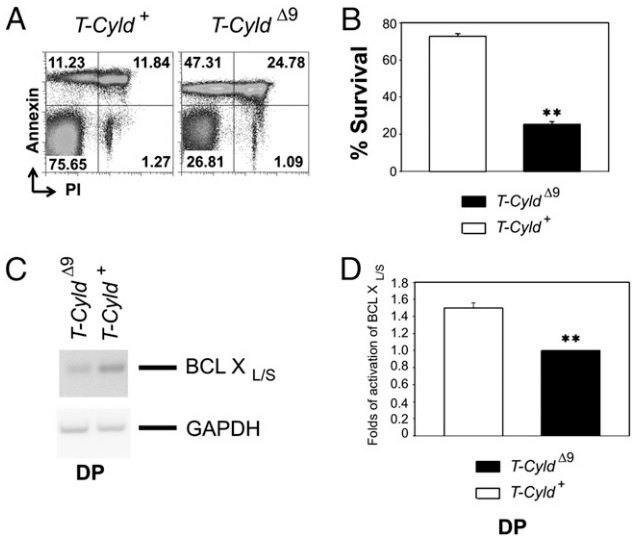

FIGURE 4. Reduced ex vivo survival of *Cyld*$^{\Delta 9}$ DP thymocytes. *A*, CD53-depleted DP thymocytes from *LckCre-Cyld*$^{flx9/+}$ (*T-Cyld*$^+$) and *LckCre-Cyld*$^{flx9/flx9}$ (*T-Cyld*$^{\Delta 9}$) mice were stained for annexin/PI and assessed by flow cytometry following their isolation and 16 h of culture. The percentages of live cells (annexin$^-$PI$^-$), early apoptotic (annexin$^+$PI$^-$), late apoptotic (annexin$^+$PI$^+$), and necrotic (annexin$^-$PI$^+$) after 16 h of culture are indicated. One representative experiment of two is depicted. At least three mice per genotype were evaluated. *B*, Enumeration of live DP thymocytes from control (*T-Cyld*$^+$) and mutant (*T-Cyld*$^{\Delta 9}$) mice after 16 h in culture as assessed in *A*. Survival of DP cells in vitro was estimated as the frequency of live cells (annexin$^-$PI$^-$) after 16 h in culture relative to the input population and represented as mean absolute numbers (± SEM) from three control (*T-Cyld*$^+$) and four mutant (*T-Cyld*$^{\Delta 9}$) mice per group at 5–6 wk of age. $^{**}p < 0.001$ indicates the statistically significant difference between the survival of control (*T-Cyld*$^+$) and mutant (*T-Cyld*$^{\Delta 9}$) mice. *C*, Reduced expression of the anti-apoptotic BCLX$_{L/S}$ in *Cyld*$^{\Delta 9}$ DP thymocytes. RT-PCR analysis using RNA isolated from CD53 depleted control (*T-Cyld*$^+$) and mutant (*T-Cyld*$^{\Delta 9}$) DP, revealed reduced expression of BCLX$_{L/S}$ in *Cyld*$^{\Delta 9}$ DP thymocytes. At least four mice per genotype were evaluated. *D*, Quantitation of BCLX$_{L/S}$ expression in *LckCre-Cyld*$^{flx9/flx9}$ (*T-Cyld*$^{\Delta 9}$) and *LckCre-Cyld*$^{flx9/+}$ (*T-Cyld*$^+$) mice. Densitometric analysis was performed, and the ratio of the BCLX $_{L/S}$ to GAPDH (expression index) was calculated. The expression index of BCLX $_{L/S}$ from purified DP thymocytes of control mice was divided by the expression index from mutant DP thymocytes, to derive the corresponding folds of upregulation of BCLX$_{L/S}$ expression.

In transgenic (*tg*)*HY*$^+$*LckCre-Cyld*$^{flx9/flx9}$ female mice, total thymic cellularity was severely reduced (Fig. 5*A*). DP thymocytes behaved similarly (data not shown). Both total thymocytes and DP thymocytes isolated from *tgHY*$^+$*LckCre-Cyld*$^{flx9/flx9}$ mice showed an even greater tendency to become apoptotic in culture relative to control HY-TCR-expressing thymocytes (Fig. 5*B* and data not shown, respectively). Thus, after 20 h of in vitro culture, the remnant *Cyld*$^{\Delta 9}$ thymocytes were reduced to almost nominal values (Fig. 5*B*, 5*C*).

Flow cytometric analysis revealed uniform expression of the transgenic HY TCR in *tgHY*$^+$*LckCre-Cyld*$^{flx9/flx9}$ thymocytes (Fig. 5*D*). Moreover, the number of DP and CD8 SP thymocytes bearing the HY TCR was reduced in *tgHY*$^+$*LckCre-Cyld*$^{flx9/flx9}$ mice (Fig. 5, *E* and *F*). However, *Cyld*$^{\Delta 9}$ CD8 SP thymocytes were mature as assessed by flow cytometric analysis of the markers CD69, CD5 and CD24 (Fig. 5*G*). More precisely, CD5 expression was increased both in DP and CD8 SP HY-expressing thymocytes, whereas both CD69 and CD24 were markedly downregulated in CD8 SP HY-expressing thymocytes. Thus, the maturation of the produced *Cyld*$^{\Delta 9}$ CD8 SP thymocytes readily takes place in this context. This finding suggests that HY TCR recognizes the Ag and that the process of positive selection is initiated. However, a large number of thymocytes that would normally be positively selected under these conditions are eliminated in the absence of functional CYLD. Collectively, our data indicate that the *Cyld*$^{\Delta 9}$ mutation leads to a change in the threshold of activation, which apparently diverts CD8 SP thymocytes from a destiny of positive selection to enhanced deletion.

Negative selection in HY male mice is characterized by severely reduced thymocyte numbers as well as nearly complete absence of DP and SP thymocytes. This profile probably reflects negative selection that occurs early in the DP stage. In HY *tgLckCre Cyld*$^{flx9/flx9}$ male mice, negative selection owing to high-affinity TCR ligand engagement takes place to the same extent as in control male mice, because the number of DP and CD8 cells were comparable (Fig. 5*H*). This finding is in accordance with the similar effect of TCR engagement on the survival of control and *LckCre Cyld*$^{flx9/flx9}$ DP thymocytes in vitro, although the interpretation of this result is compromised by the much greater tendency of *LckCre Cyld*$^{flx9/flx9}$ DP thymocytes to undergo apoptosis (Supplemental Fig. 5).

To further evaluate the implication of CYLD in positive selection of CD4 lineage, we crossed *LckCre-Cyld*$^{flx9/flx9}$ mice with the OT-2 TCR transgenic mice that express a TCR composed of V a2/V β5 chains, recognizing the OVA peptide 323–339 in the context of MHC class II I-Ab (32). The analysis indicated a severe reduction in total thymic cellularity of *tgOT2*$^+$ *LckCre-Cyld*$^{flx9/flx9}$ mice compared with control mice (Fig. 6*A*) that was accompanied by a decrease in the ex vivo survival of thymocytes (Fig. 6*B*). Moreover, there was an apparent reduction in TCR expression (Fig. 6*C*) that, combined with the absence of CD4 T cells in the Va2/Vβ5 TCR high thymocytes, reveals that positive selection is completely abolished in the absence of functional CYLD protein (Fig. 6*D*, 6*E*). Furthermore, *tgOT2*$^+$ *LckCre-Cyld*$^{flx9/flx9}$ mice had a tendency to lose CD4$^+$CD8^{lo} thymocytes, which represent an intermediate population that has initiated selection in response to

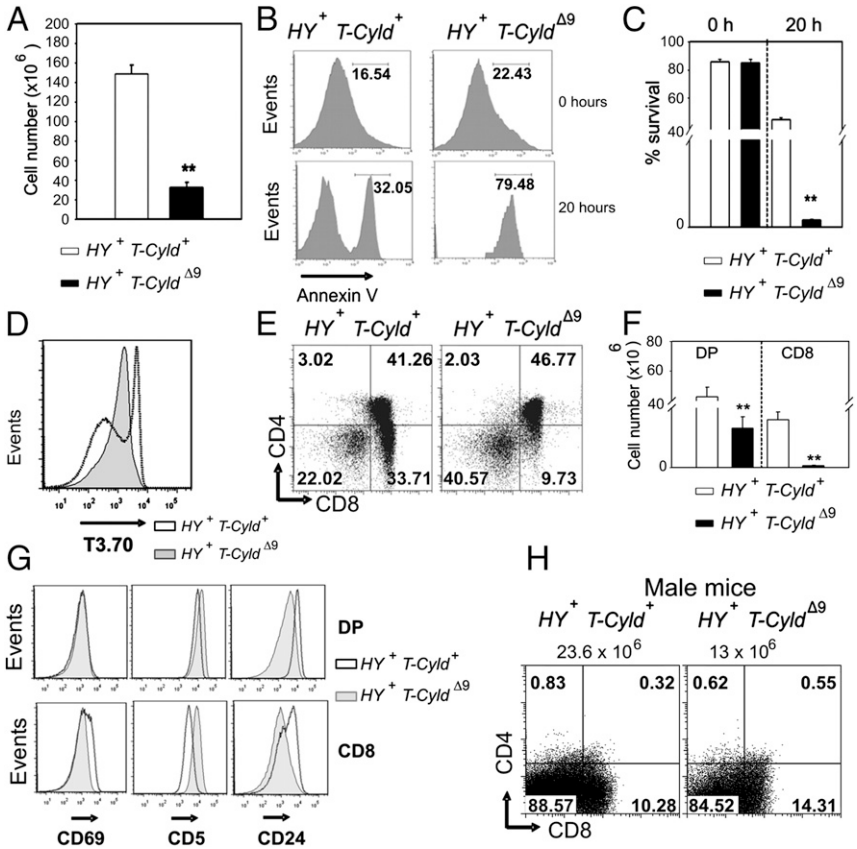

FIGURE 5. Impaired positive selection in *LckCreCyld*$^{flx9/flx9}$ MHC class I restricted transgenic mice. *A*, Total thymocyte number in female control (*tgHY*$^+$ *LckCre-Cyld*$^{flx9/+}$ [*HY*$^+$ *T-Cyld*$^+$]) and mutant (*tgHY*$^+$ *LckCre-Cyld*$^{flx9/flx9}$ [*HY*$^+$ *T-Cyld*$^{\Delta 9}$]) mice. Data are depicted as mean absolute numbers (± SEM) from $n = 7$–9 mice per group. $^{**}p = 0.001$ indicates the statistically significant difference in the total number of thymocytes between control (*HY*$^+$ *T-Cyld*$^+$) and mutant (*HY*$^+$ *T-Cyld*$^{\Delta 9}$) mice. *B*, Histograms depicting annexin V staining in PI$^-$ fresh (0 h) or cultured (for 20 h) thymocytes from control (*HY*$^+$ *T-Cyld*$^+$) and mutant (*HY*$^+$ *T-Cyld*$^{\Delta 9}$) mice . *C*, In vitro survival of fresh and cultured thymocytes isolated from two control (*HY*$^+$ *T-Cyld*$^+$) and three mutant (HY$^+$ *T-Cyld*$^{\Delta 9}$) mice. Average values ± SE are shown. $^{**}p < 0.00024$ indicates statistically significant differences. *D*, Representative histogram depicting the difference in the expression of the HY-TCR (T3.70) between total thymocytes from control ([*HY*$^+$ *T-Cyld*$^+$], open histogram) and mutant ([*HY*$^+$ *T-Cyld*$^{\Delta 9}$], shaded histogram) mice. *E*, Representative subset distribution of gated HY-TCR–expressing thymocytes by means of CD4 and CD8 expression in control (*HY*$^+$ *T-Cyld*$^+$) and mutant (*HY*$^+$ *T-Cyld*$^{\Delta 9}$) mice. *F*, Enumeration of HY-TCR–expressing DP and CD8$^+$ thymocytes in control (*HY*$^+$ *T-Cyld*$^+$) and mutant (*HY*$^+$ *T-Cyld*$^{\Delta 9}$) mice. Data are depicted as mean absolute numbers (± SEM) from $n = 7$–9 mice per group. $^{**}p = 0.0005$; $^{**}p = 0.0006$ indicate the statistically significant differences in DP and CD8 thymocytes between control and mutant mice, respectively. *G*, Representative histograms that depict the expression of CD69, CD5, and CD24 in both DP and CD8 SP that express HY-TCR in control ([*HY*$^+$ *T-Cyld*$^+$], open histogram) and mutant ([*HY*$^+$ *T-Cyld*$^{\Delta 9}$], shaded histogram) mice. If not otherwise stated, data are representative of at least three independent experiments. *H*, Analysis of CD4 and CD8 thymic subsets in male control (*HY*$^+$ *T-Cyld*$^+$) and mutant (*HY*$^+$ *T-Cyld*$^{\Delta 9}$) mice by flow cytometry. Thymocytes expressing high levels of T3.70-reactive TCR were evaluated for CD4 and CD8 expression. Data from one representative experiment of three are depicted. Three 6-wk-old mice per genotype were evaluated.

TCR signaling and are midway in the transition from DP to SP cells (Fig. 6*D*, 6*E*) (27). However, *Cyld*$^{\Delta 9}$ DP thymocytes with Va2/Vβ5 TCR high expression upregulated CD5 and CD69 similarly to control DP thymocytes, whereas they downregulated CD24 more prominently than control DP thymocytes, a sign of premature maturation (Fig. 6*F*) (33). Moreover, flow cytometric analysis of the spleen (Fig. 6*G*, 6*H*) and mesenteric lymph nodes (data not shown) of TCR Vβ5 and CD4 expression revealed a nearly complete absence of peripheral T cells. These data establish CYLD as a key player in the positive selection of the CD4 lineage, most likely by maintaining a proper threshold of activation and thus safeguarding the outcome of positive selection.

Aberrant activation of NF-κB and JNK in Cyld$^{\Delta 9}$ *thymocytes*

It has been shown previously that CYLD is a negative regulator of NF-κB and JNK. This finding prompted an investigation of the activity of the two pathways in *Cyld*$^{\Delta 9}$ thymocytes. Importantly, basal levels of NF-κB DNA-binding activity were dramatically increased in *Cyld*$^{\Delta 9}$ thymocytes compared with control thymocytes (Fig. 7*A*, *upper panel*, compare *lanes 3* and *4*). The activity of NF-κB was mainly due to the binding of p65 and p50 subunits (Fig. 7*A*, upper panel, *lane 6* and data not shown). Similar results were obtained with nuclear extracts from DP thymocytes (Supplemental Fig. 4*B*, compare *lanes 3* and *4*). In addition, the activity of JNK was also elevated in *Cyld*$^{\Delta 9}$ thymocytes compared with control thymocytes (Fig. 7*B*, compare *lanes 2* and *3* and Fig. 7*C*). These findings implicate the deregulated activation of NF-κB and JNK in defective *Cyld*$^{\Delta 9}$ thymocyte selection.

Inactivation of NEMO rescues the developmental defects of Cyld$^{\Delta 9}$ *thymocytes*

CYLD has been shown to interact with NEMO, which plays a fundamental role in the activation of NF-κB as an integral component of the I-κB kinase (IKK) complex (2, 3). More recently, NEMO has been implicated in the activation of JNK (34, 35). To determine whether NEMO is involved in the defective selection of

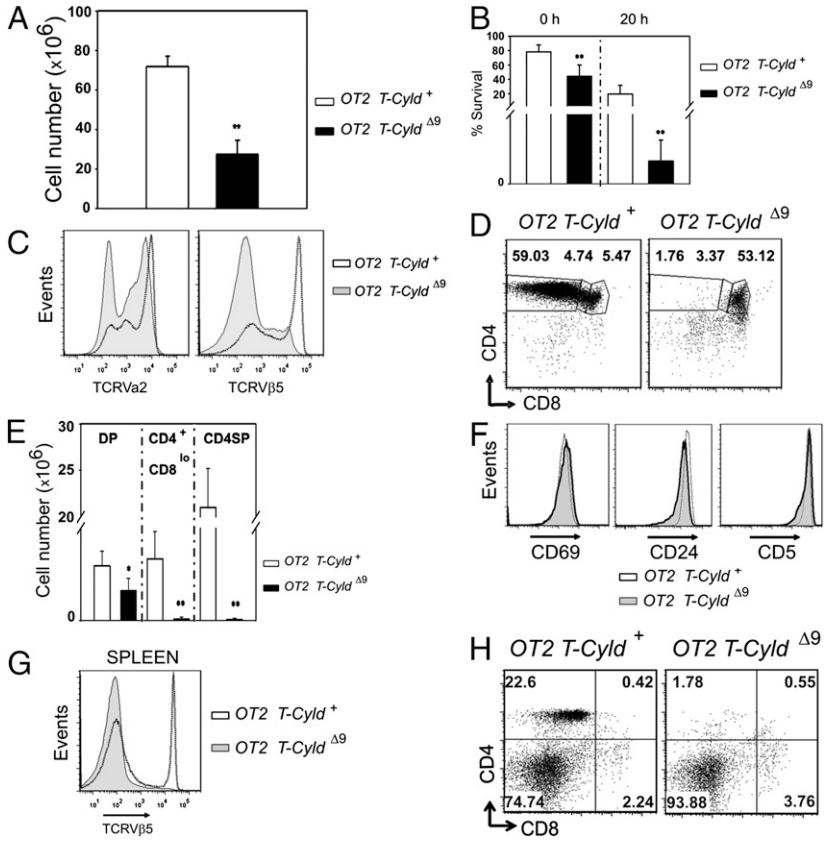

FIGURE 6. Positive selection of MHC class II-restricted TCR transgenic mice was practically abolished in $Cyld^{\Delta 9}$ T cells. *A*, Total thymocyte number in female control (*tgOT2 LckCre-Cyld*$^{flx9/+}$ [*OT2 T-Cyld*$^{+}$]) and mutant (*tgOT2 LckCre-Cyld*$^{flx9/flx9}$ [*OT2 T-Cyld*$^{\Delta 9}$]) mice. Data are depicted as mean absolute numbers (± SEM) from $n = 5$ mice per group. $^{**}p = 0.001$ indicates the statistically significant difference in the total number of thymocytes between control and mutant mice. *B,* In vitro survival of fresh and cultured thymocytes isolated from seven control (*OT2 T-Cyld*$^{+}$) and five mutant (*OT2 T-Cyld*$^{\Delta 9}$) mice. Average values ± SE are shown. $^{**}p < 0.008$ indicates statistically significant differences. *C*, Impaired positive selection in *OT2 T-Cyld*$^{\Delta 9}$ mice as assessed by their inability to upregulate TCRVβ. Representative histograms are shown for the surface expression of TCRVα and TCRVβ. The open histogram represents control mice, whereas the shaded histogram represents mutant mice. At least seven mice per genotype were evaluated. Data are representative of three separate experiments. *D*, Representative subset distribution of gated TCRVβ2/Vα5-expressing thymocytes by means of CD4 and CD8 expression in control (*OT2 T-Cyld*$^{+}$) and mutant (*OT2 T-Cyld*$^{\Delta 9}$) mice. *E*, Absolute numbers of DP, CD4^{+}CD8^{lo}, and CD4 SP in TCRVα2/Vβ5 gated thymocytes from control (*OT2 T-Cyld*$^{+}$) and mutant (*OT2 T-Cyld*$^{\Delta 9}$) mice. Data are depicted as mean absolute numbers (± SEM) from $n = 5$ mice per group. At least two independent experiments were performed. $^{*}p = 0.031$; $^{**}p = 0.003$; $^{**}p = 0.001$ indicate the statistically significant differences in DP, CD4^{+}CD8^{lo}, and CD4 thymocytes between control and mutant mice, respectively. *F,* Representative histograms that depict the expression of CD69, CD5, and CD24 in gated TCRVα2/Vβ5-expressing DP in control (*OT2 T-Cyld*$^{+}$, open histogram) and mutant (*OT2 T-Cyld*$^{\Delta 9}$, shaded histogram) mice. *G*, Representative histograms that depict the surface expression of TCR Vβ2 in splenocytes isolated from control (*OT2 T-Cyld*$^{+}$, open histogram) and mutant (*OT2 T-Cyld*$^{\Delta 9}$, shaded histogram) mice. At least five mice per genotype were evaluated. *H*, Surface expression of CD4 and CD8 in splenocytes from control (*OT2 T-Cyld*$^{+}$) and mutant (*OT2 T-Cyld*$^{\Delta 9}$) mice. $n = 5$ mice per genotype. In all cases, data are representative of at least two independent experiments.

thymocytes in *LckCre-Cyld*$^{flx9/flx9}$ mice, these mice were crossed with mice (*Nemo*^{flx}) carrying a conditionally-targeted *Nemo* allele. More specifically, *Nemo*^{flx} mice bear a premature stop codon that can be conditionally introduced in a Cre-dependent manner and have been used already to evaluate the function of NEMO in T cell development (21). The double mutant mice (*LckCre-Cyld*$^{flx9/flx9}$-*Nemo*^{flx}) were viable and fertile and showed no obvious abnormalities. The loxP-targeted *Nemo* and *Cyld* alleles were efficiently recombined in the thymocytes of *LckCre-Cyld*$^{flx9/flx9}$-*Nemo*^{flx} mice, as determined by competitive genomic PCR (Supplemental Fig. 6*A*, 6*B*). It should be noted that the recombination efficiency of the *Cyld*^{flx9} allele in *LckCre-Cyld*$^{flx9/flx9}$-*Nemo*^{flx} mice was comparable to its recombination in *LckCre-Cyld*$^{flx9/flx9}$ mice (Supplemental Fig. 6*B*). Furthermore, the efficient recombination of the *Cyld*^{flx9} allele was confirmed by the absence of a full-length *Cyld* transcript and the expression of a *Cyld*$^{\Delta 9}$ transcript in DP thymocytes from mice (Supplemental Fig. 6*C*). Finally, full-length CYLD protein was undetectable (Supplemental Fig. 6*D*), and NEMO was significantly reduced, in accordance with previous reports (36), in thymocytes from *LckCre-Cyld*$^{flx9/flx9}$-*Nemo*^{flx} double mutant mice as determined by immunoblotting (Supplemental Fig. 6*E*). Concomitant inactivation of NEMO in thymocytes with mutated *Cyld* fully restored the basal activity of NF-κB to physiologic levels (Fig. 7*A*, compare *lanes* 2, *3*, and *4*) and attenuated JNK activation, which remained above physiologic levels (Fig. 7*B*, compare *lanes 1*, *2*, *3*, and Fig. 7*C*). Most importantly, both CD4 and CD8 SP populations in mice with mutated *Cyld* and *Nemo* were restored to levels that were comparable to those seen in control mice (Fig. 8*A*, 8*B*). Nevertheless, the absolute number of CD8 SP in the double mutants was lower than the corresponding population of control mice, a finding that can be attributed to *Nemo* deficiency as previously described (Fig. 8*B*) (36). Furthermore, and in accordance with the previously described phenotype of mice with T cell-specific *Nemo* deficiency, CD8 SP thymocytes from double mutant mice showed an immature phenotype, as reflected by their inability to downregulate CD24 (data not shown), whereas in the periphery

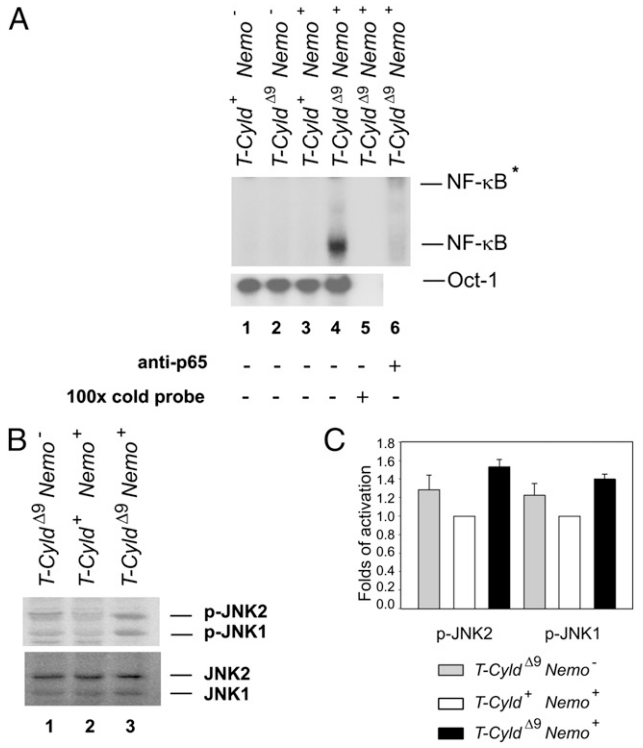

FIGURE 7. Elevated basal activity of NF-κB and JNK in *Cyld*$^{\Delta 9}$ thymocytes. *A*, EMSA of NF-κB and Oct-1 DNA binding activity in thymocytes from *LckCre-Cyld*$^{+/+}$ *Nemo*$^{flx/flx}$ (*T-Cyld*$^{+}$ *Nemo*$^{-}$), *LckCre-Cyld*$^{flx9/flx9}$ *Nemo*$^{flx/flx}$ (*T-Cyld*$^{\Delta 9}$ *Nemo*$^{-}$), *LckCre-Cyld*$^{flx9/+}$ *Nemo*$^{+}$ (*T-Cyld*$^{+}$ *Nemo*$^{+}$), and *LckCre-Cyld*$^{flx9/flx9}$ *Nemo*$^{+}$ (*T-Cyld*$^{\Delta 9}$ *Nemo*$^{+}$) mice in the absence or presence of a 100-fold excess of unlabeled probe (100× cold probe) or anti-p65 Ab as indicated. The positions of Oct-1– and NF-κB–containing complexes of the radiolabeled probe are shown. The position of the NF-κB–containing complex that is supershifted by the anti-p65 Ab is shown by an asterisk. One representative of three independent experiments is shown. At least three mice per genotype were evaluated. *B*, Immunobloting of phosphorylated and total JNK in thymocytes from *LckCre-Cyld*$^{flx9/flx9}$*Nemo*$^{flx/flx}$ (*T-Cyld*$^{\Delta 9}$ *Nemo*$^{-}$), *LckCre-Cyld*$^{flx9/+}$ *Nemo*$^{+}$ (*T-Cyld*$^{+}$ *Nemo*$^{+}$), and *LckCre-Cyld*$^{flx9/flx9}$ *Nemo*$^{+}$ (*T-Cyld*$^{\Delta 9}$ *Nemo*$^{+}$) mice (*left panel*). One representative experiment of two is depicted. At least two mice per genotype were evaluated. *C*, Quantitation of JNK1 and JNK2 activity in *LckCre-Cyld*$^{flx9/flx9}$ *Nemo*$^{flx/flx}$ (*T-Cyld*$^{\Delta 9}$ *Nemo*$^{-}$), *LckCre-Cyld*$^{flx9/+}$ *Nemo*$^{+}$ (*T-Cyld*$^{+}$ *Nemo*$^{+}$), and *LckCre-Cyld*$^{flx9/flx9}$ *Nemo*$^{+}$ (*T-Cyld*$^{\Delta 9}$ *Nemo*$^{+}$) mice. Densitometric analysis was performed, and the ratio of the phosphorylated JNK1 to total JNK1 (activity index) was calculated. The same procedure was followed for JNK2. The activity indexes of JNK1 and JNK2 from thymocytes of double-mutant and single-mutant mice were divided by the activity indexes of JNK1 and JNK2 from control thymocytes, respectively, to derive the corresponding folds of activation. Data are depicted as mean absolute numbers (± SEM) from $n = 2$ mice per group at 5–6 wk of age.

both CD4^{+} and CD8^{+} T cells were dramatically reduced (Supplemental Fig. 6*G*, 6*H*), because proper NF-κB activity is required for the survival of mature T cells (36).

Further analysis showed that double mutants and control mice had comparable numbers of mature SP thymocytes (TCRβ^{hi}CD24^{lo}) (Fig. 8*C*, 8*D*), and the double mutant DP cells were able to complete the process of positive selection, as assessed by the combined expression of TCRβ with CD69 (Fig. 8*E*, 8*F*) or CD5 (Supplemental Fig. 6*F*). A slight reduction in CD24 mean fluorescence intensity was noted in the CD24^{hi}TCRβ$^{int/lo}$ subset of double mutant DP thymocytes compared with the corresponding population of control DP thymocytes, although the basis for this minor difference is unclear. Finally, the survival of thymocytes in double mutant mice was completely restored (data not shown). Our results establish a functional interplay between CYLD and NEMO in the orchestration of thymocyte selection by setting the optimal threshold of activation.

Discussion

The implication of *Cyld* in the regulation of mammalian immune responses and the controversy that surrounds the role of *Cyld* in thymocyte development and activation prompted an investigation of the specific function of *Cyld* in thymocytes. For this purpose, a conditional gene targeting approach permitted the inactivation of CYLD's activity from the early stages of thymocyte development onward in a manner that mimics the naturally occurring mutations of *Cyld* in humans. The mating of mice with floxed *Cyld* exon 9 to *LckCre* mice resulted in efficient and specific elimination of *Cyld* exon 9 in thymocytes. Interestingly, the thymocyte-specific excision of *Cyld* exon 9 resulted in a dramatic decrease of both CD4^{+} and CD8^{+} SP thymocyte populations. Our results are consistent with a previous study by Reiley et al. (15) that analyzed mice with complete inactivation of *Cyld* in all tissues that resulted in the reduction of SP thymocytes. However, our approach analyzed the role of CYLD specifically in thymocytes, and it demonstrated a thymocyte-intrinsic requirement of functional CYLD for the positive selection of SP thymocytes. Our attempt to further elucidate the function of CYLD in the multifaceted procedure of DP selection uncovered an unexpected feature. More precisely, the use of *Cyld*-deficient TCR transgenic mice revealed increased death and dramatic reduction of thymic cellularity in an environment that otherwise favors the process of positive selection, as manifested also by the proper upregulation of positive selection markers. These data are consistent with defective positive selection in *Cyld*-deficient thymocytes.

Reiley et al. (15) associated the developmental defect of *Cyld*-null thymocytes with impaired proximal TCR signaling, which was traced to suboptimal activation of Zap70. In our mouse model of *Cyld*-deficiency, we could not detect a significant impairment in the early stages of TCR signaling, as assessed by the activation of Lck, Zap70, and LAT (Supplemental Fig. 4*A*). This finding is consistent with the ability of *Cyld*$^{\Delta 9}$ DP thymocytes to initiate the process of positive selection. The difference between our study and the study of Reiley et al. (15) in proximal TCR signaling of *Cyld*-deficient thymocytes could be attributed to the different gene-targeting strategy. Although our data cannot be used to exclude a potential contribution of CYLD in TCR signaling, our genetic analysis revealed a dominant regulatory effect of NEMO-dependent signaling in optimal selection of *Cyld*-deficient thymocytes. An obvious issue for consideration is the molecular nature of the functional interaction between CYLD and NEMO. A physical interaction between these two molecules has been established by previous studies (2, 3). Alternatively, NEMO ubiquitination and/or its ability to interact with polyubiquitin chains has been associated with the activation of the NF-κB and JNK pathways, and it has been shown that CYLD can mediate the deubiquitination of NEMO (3, 34, 35, 37, 38). More recently, the interaction of NEMO with free polyubiquitin chains has been shown to mediate the activation of IKK in vitro, and CYLD could inhibit this process by disassembling the unanchored polyubiquitin chains (39). These data provide a molecular framework of the functional relationship between CYLD and NEMO, which is based on the ability of CYLD to inhibit the activity of NEMO directly or indirectly in a deubiquitination-dependent manner.

Thymocyte-specific inactivation of CYLD led to an aberrant activation of NF-κB and JNK. A concomitant ablation of NEMO in

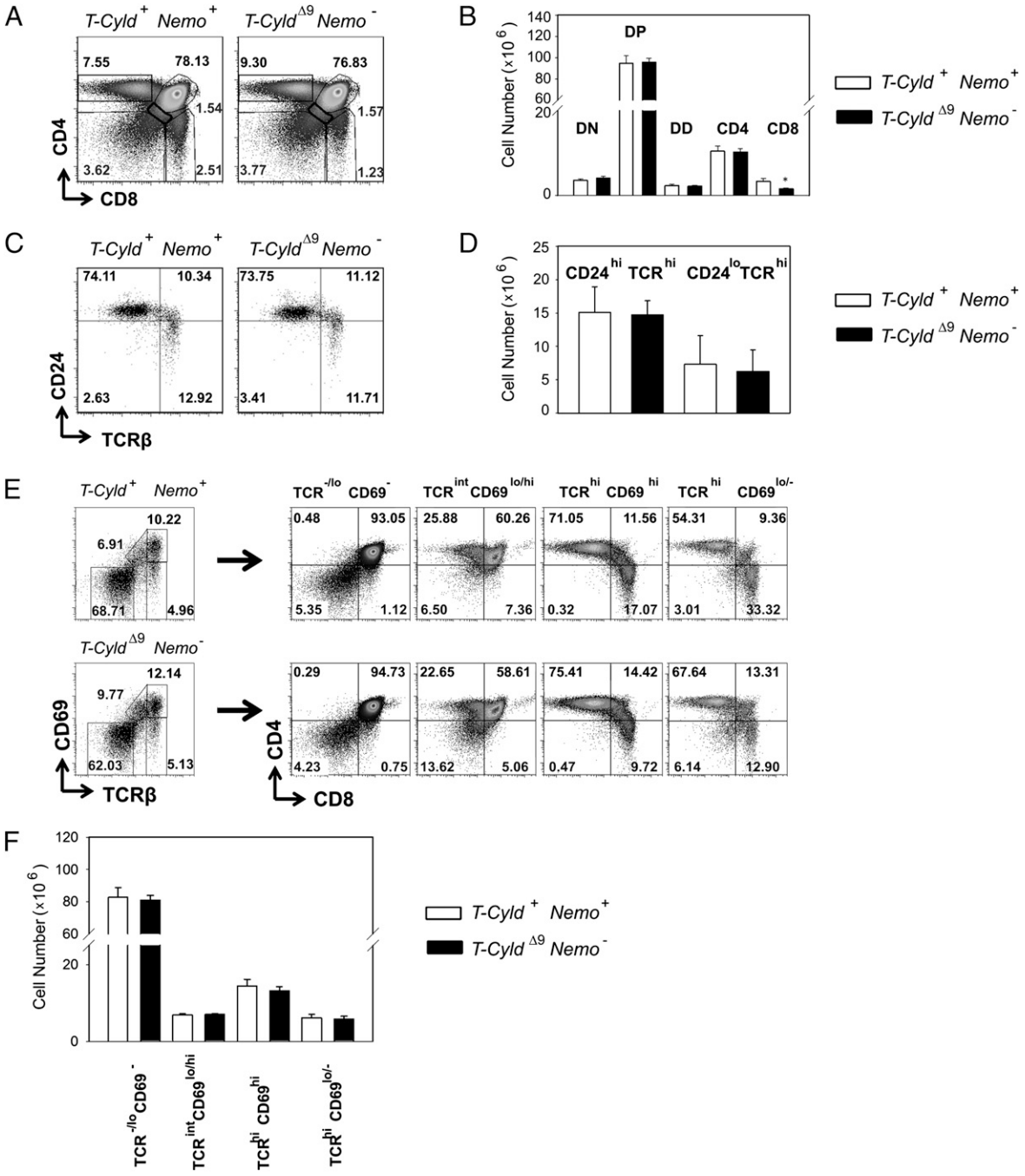

FIGURE 8. Rescue of the main developmental defects of *T-Cyld*$^{\Delta 9}$ by genetic ablation of *Nemo*. *A*, Representative subset distribution of thymocytes derived from control (*LckCre-Cyld*$^{flx9/+}$ *Nemo*$^{+}$ [*T-Cyld*$^{+}$ *Nemo*$^{+}$]) and double mutant (*LckCre-Cyld*$^{flx9/flx9}$ *Nemo*$^{-}$ [*T-Cyld*$^{\Delta 9}$ *Nemo*$^{-}$]) mice by means of CD4 and CD8 expression. *B*, Enumeration of thymocyte subsets as assessed in *A*. Data are depicted as mean absolute numbers (± SEM) from $n = 5$ mice per group at 5–6 wk of age. $*p = 0.048$, the statistically significant difference in CD8^{+} thymocytes between control (*T-Cyld*$^{+}$ *Nemo*$^{+}$) and double mutant (*T-Cyld*$^{\Delta 9}$ *Nemo*$^{-}$) mice. *C*, Representative flow cytometric detection by means of CD24 and TCRβ expression from control (*T-Cyld*$^{+}$ *Nemo*$^{+}$) and double mutant (*T-Cyld*$^{\Delta 9}$ *Nemo*$^{-}$) mice. *D*, Enumeration of CD24- and TCRβ-defined thymic subsets as assessed in *C*. Data are depicted as mean absolute numbers (± SEM) from $n = 5$ mice per group at 5–6 wk of age. *E*, Representative flow cytometric detection of CD69 and TCRβ expression in total thymocytes from control (*T-Cyld*$^{+}$ *Nemo*$^{+}$) and double mutant (*T-Cyld*$^{\Delta 9}$ *Nemo*$^{-}$) mice (*left panels*). Defined subsets representing distinct developmental stages (TCRβ$^{-/lo}$ CD69^{-}, TCR^{int}CD69$^{lo/hi}$, TCR^{hi}CD69^{hi}, and TCR^{hi}CD69$^{lo/-}$) were further analyzed for CD4 and CD8 expression (*right panels*, indicated by arrows). *F*, Enumeration of thymic subsets from control (*T-Cyld*$^{+}$ *Nemo*$^{+}$) and double mutant (*T-Cyld*$^{\Delta 9}$ *Nemo*$^{-}$) mice as defined by the expression of TCR and CD69 in *E*. Data are depicted as mean absolute numbers (± SEM) from $n = 5$ mice per group at 5–6 wk of age. In all cases, data are representative of at least two independent experiments.

Cyld-deficient thymocytes essentially rescued their developmental defects and fully restored the activity of NF-κB to physiologic levels, whereas it partially reduced the activity of JNK, which remained above physiologic levels. Our findings indicate that aberrant activation of NF-κB and possibly JNK mediate a derailment of *Cyld*-deficient thymocyte development from a physiological process of positive selection to elimination, which could be attributed, at least in part, to surpassing of appropriate thresholds of activation. Our results are in agreement with the findings of Jimi et al. (33), who demonstrated loss of SP thymocytes in a transgenic

mouse model of NF-κB–hyperactivation that overexpresses constitutively active IKK2. Similar to our study, Jimi et al. (33) provide evidence that attributes the loss of SP thymocytes to conversion of positive to negative selection because of aberrantly elevated NF-κB activity. Nevertheless, our study, which did not rely on an artificial upregulation of an integral NF-κB pathway component, identified CYLD as a functionally important inhibitor of NF-κB in thymocytes and an apparent master regulator of thresholds of thymocyte activation that orchestrate their proper selection process. A proapoptotic role of NF-κB in DP thymocytes has been suggested also by the increased resistance to CD3-mediated apoptosis by DP thymocytes expressing a nondegradable form of IκBα (29). The antiapoptotic behavior of NF-κB–deficient DP thymocytes was attributed to increased $BCLX_{L/S}$ expression. Interestingly, $Cyld^{\Delta 9}$ thymocytes exhibit decreased $BCLX_{L/S}$ expression (Fig. 4*C*, 4*D*), highlighting a plausible molecular mechanism for their increased deletion. In addition, our results provide critical information for the clarification of the emerging role of NF-κB in SP thymocyte development. Jimi et al. (33) established NF-κB activation as a key event in CD8 development, a finding that is in accordance with the defective production of CD8 SPs in mice with thymocyte-specific IKK2 deficiency (40). Moreover, they showed that NF-κB activity increases in $CD69^+$ DP thymocytes, which represent the subpopulation of DP thymocytes that undergoes positive selection, whereas $CD69^-$ DP thymocytes have practically undetectable NF-κB activity. These observations support a regulatory role of NF-κB activity during selection-associated DP thymocyte activation with optimal NF-κB activation being apparently important for the initial transition of DP to CD8 SP thymocytes and its downregulation having a critical role in the establishment of the CD4 lineage (33). Intriguingly, expression of CYLD is higher in SP thymocytes (15), suggesting a major role of CYLD in the ontogeny of these subsets. The following scenario could be envisaged. $Cyld^{\Delta 9}$ DP thymocytes have an abnormally high basal level of NF-κB activity, which increases further as DP cells enter the process of Ag-dependent positive selection. As DP thymocytes proceed toward the completion of positive selection the lack of functional CYLD impairs the fine tuning of NF-κB activity, and its levels remain extremely high. The hyperactivation of NF-κB is detrimental for $CD4^+CD8^{lo}$ cells where NF-κB must be downregulated and this may also explain why CD4 SP cells are apparently more affected than CD8 SP. Alternatively, $Cyld^{\Delta 9}$ CD8 SP are also reduced, albeit to a lesser extent than CD4 SP, because in the absence of functional CYLD NF-κB activity reaches higher levels than the optimal ones for positive selection, possibly leading to their deletion. Interestingly, the process of negative selection by high-affinity self ligands in HY male mice did not differ between $Cyld^{\Delta 9}$ and control thymocytes. Apparently, the increased activity of NF-κB in *Cyld*-deficient thymocytes does not influence the outcome of the abnormally high level of TCR signaling after the engagement of HY Ag in HY tg *LckCre* $Cyld^{flx9/flx9}$ male mice. This finding is in accordance with the results of Jimi et al. (33).

The differential requirement of NF-κB activity for the development of CD8 and CD4 thymocytes may underlie a possible crosstalk of NF-κB with lineage commitment factors. More specifically, NF-κB could interfere with the activity of the transcription factor Runx3, which governs the process of CD8 lineage commitment by binding and activating the CD8 enhancer and also by suppressing CD4 expression through the CD4 silencer in CD8 SPs (41, 42). Furthermore, NF-κB may also regulate the activity of ThPOK, which is required in MHC II selected thymocytes to prevent Runx-dependent differentiation toward the CD8 lineage (43).

In addition to NF-κB, a potential role for JNK in setting appropriate thresholds of thymocyte activation would be also consistent with our findings. This notion is also supported by previous work by Rincón et al. (44), who demonstrated that forced inhibition of JNK protects thymocytes from CD3-mediated deletion, indicating that JNK activation is implicated in the process of thymocyte deletion and negative selection.

Our results establish a thymocyte-intrinsic role of CYLD in the positive selection of SP thymocytes and the maturation of T cells by fine tuning of NEMO-dependent signaling pathways. Undoubtedly, the detailed characterization of the NEMO-dependent gene-expression program that is regulated by CYLD in the thymus will illuminate important aspects of the complex mechanism of thymocyte development and maturation.

Acknowledgments

We thank Dr. Shao-Cong Sun (The University of Texas MD Anderson Cancer Center, Houston, TX) for reagents, Dr. Manolis Pasparakis (University of Cologne, Cologne, Germany) for $Nemo^{flx}$ mice, Dr. Olympia Papadaki (Biomedical Sciences Research Center Alexander Fleming, Vari, Greece) for technical assistance, Dr. Marios Agelopoulos (Columbia University, New York, NY) for inspiring discussions, and Dr. Clio Mamalaki (Institute of Molecular Biology and Biotechnology, Heraklion, Greece) for critical reading of the manuscript.

Disclosures

The authors have no financial conflict of interest.

References

1. Borodovsky, A., H. Ovaa, N. Kolli, T. Gan-Erdene, K. D. Wilkinson, H. L. Ploegh, and B. M. Kessler. 2002. Chemistry-based functional proteomics reveals novel members of the deubiquitinating enzyme family. *Chem. Biol.* 9: 1149–1159.
2. Trompouki, E., E. Hatzivassiliou, T. Tsichritzis, H. Farmer, A. Ashworth, and G. Mosialos. 2003. CYLD is a deubiquitinating enzyme that negatively regulates NF-kappaB activation by TNFR family members. *Nature* 424: 793–796.
3. Kovalenko, A., C. Chable-Bessia, G. Cantarella, A. Israël, D. Wallach, and G. Courtois. 2003. The tumour suppressor CYLD negatively regulates NF-kappaB signalling by deubiquitination. *Nature* 424: 801–805.
4. Bignell, G. R., W. Warren, S. Seal, M. Takahashi, E. Rapley, R. Barfoot, H. Green, C. Brown, P. J. Biggs, S. R. Lakhani, et al. 2000. Identification of the familial cylindromatosis tumour-suppressor gene. *Nat. Genet.* 25: 160–165.
5. Hellerbrand, C., E. Bumes, F. Bataille, W. Dietmaier, R. Massoumi, and A. K. Bosserhoff. 2007. Reduced expression of CYLD in human colon and hepatocellular carcinomas. *Carcinogenesis* 28: 21–27.
6. Zhong, S., C. R. Fields, N. Su, Y. X. Pan, and K. D. Robertson. 2007. Pharmacologic inhibition of epigenetic modifications, coupled with gene expression profiling, reveals novel targets of aberrant DNA methylation and histone deacetylation in lung cancer. *Oncogene* 26: 2621–2634.
7. Keats, J. J., R. Fonseca, M. Chesi, R. Schop, A. Baker, W. J. Chng, S. Van Wier, R. Tiedemann, C. X. Shi, M. Sebag, et al. 2007. Promiscuous mutations activate the noncanonical NF-kappaB pathway in multiple myeloma. *Cancer Cell* 12: 131–144.
8. Annunziata, C. M., R. E. Davis, Y. Demchenko, W. Bellamy, A. Gabrea, F. Zhan, G. Lenz, I. Hanamura, G. Wright, W. Xiao, et al. 2007. Frequent engagement of the classical and alternative NF-kappaB pathways by diverse genetic abnormalities in multiple myeloma. *Cancer Cell* 12: 115–130.
9. Jenner, M. W., P. E. Leone, B. A. Walker, F. M. Ross, D. C. Johnson, D. Gonzalez, L. Chiecchio, E. Dachs Cabanas, G. P. Dagrada, M. Nightingale, et al. 2007. Gene mapping and expression analysis of 16q loss of heterozygosity identifies WWOX and CYLD as being important in determining clinical outcome in multiple myeloma. *Blood* 110: 3291–3300.
10. Courtois, G. 2008. Tumor suppressor CYLD: negative regulation of NF-kappaB signaling and more. *Cell. Mol. Life Sci.* 65: 1123–1132.
11. Sun, S. C. 2009. CYLD: a tumor suppressor deubiquitinase regulating NF-kappaB activation and diverse biological processes. *Cell Death Differ.* 17: 25–34.
12. Massoumi, R. 2010. Ubiquitin chain cleavage: CYLD at work. *Trends Biochem. Sci.* DOI:10.1016/j.tibs.2010.02.007.
13. Costello, C. M., N. Mah, R. Häsler, P. Rosenstiel, G. H. Waetzig, A. Hahn, T. Lu, Y. Gurbuz, S. Nikolaus, M. Albrecht, et al. 2005. Dissection of the inflammatory bowel disease transcriptome using genome-wide cDNA microarrays. *PLoS Med.* 2: e199.
14. Reiley, W. W., W. Jin, A. J. Lee, A. Wright, X. Wu, E. F. Tewalt, T. O. Leonard, C. C. Norbury, L. Fitzpatrick, M. Zhang, and S. C. Sun. 2007. Deubiquitinating enzyme CYLD negatively regulates the ubiquitin-dependent kinase Tak1 and prevents abnormal T cell responses. *J. Exp. Med.* 204: 1475–1485.
15. Reiley, W. W., M. Zhang, W. Jin, M. Losiewicz, K. B. Donohue, C. C. Norbury, and S. C. Sun. 2006. Regulation of T cell development by the deubiquitinating enzyme CYLD. *Nat. Immunol.* 7: 411–417.

16. Zhang, J., B. Stirling, S. T. Temmerman, C. A. Ma, I. J. Fuss, J. M. Derry, and A. Jain. 2006. Impaired regulation of NF-kappaB and increased susceptibility to colitis-associated tumorigenesis in CYLD-deficient mice. *J. Clin. Invest.* 116: 3042–3049.
17. Jin, W., W. R. Reiley, A. J. Lee, A. Wright, X. Wu, M. Zhang, and S. C. Sun. 2007. Deubiquitinating enzyme CYLD regulates the peripheral development and naive phenotype maintenance of B cells. *J. Biol. Chem.* 282: 15884–15893.
18. Hövelmeyer, N., F. T. Wunderlich, R. Massoumi, C. G. Jakobsen, J. Song, M. A. Wörns, C. Merkwirth, A. Kovalenko, M. Aumailley, D. Strand, et al. 2007. Regulation of B cell homeostasis and activation by the tumor suppressor gene CYLD. *J. Exp. Med.* 204: 2615–2627.
19. Trompouki, E., A. Tsagaratou, S. K. Kosmidis, P. Dollé, J. Qian, D. L. Kontoyiannis, W. V. Cardoso, and G. Mosialos. 2009. Truncation of the catalytic domain of the cylindromatosis tumor suppressor impairs lung maturation. *Neoplasia* 11: 469–476.
20. Orban, P. C., D. Chui, and J. D. Marth. 1992. Tissue- and site-specific DNA recombination in transgenic mice. *Proc. Natl. Acad. Sci. USA* 89: 6861–6865.
21. Schmidt-Supprian, M., W. Bloch, G. Courtois, K. Addicks, A. Israël, K. Rajewsky, and M. Pasparakis. 2000. NEMO/IKK gamma-deficient mice model incontinentia pigmenti. *Mol. Cell* 5: 981–992.
22. Reiley, W., M. Zhang, and S. C. Sun. 2004. Negative regulation of JNK signaling by the tumor suppressor CYLD. *J. Biol. Chem.* 279: 55161–55167.
23. Tanchot, C., A. Le Campion, B. Martin, S. Léaument, N. Dautigny, and B. Lucas. 2002. Conversion of naive T cells to a memory-like phenotype in lymphopenic hosts is not related to a homeostatic mechanism that fills the peripheral naive T cell pool. *J. Immunol.* 168: 5042–5046.
24. Voehringer, D., H. E. Liang, and R. M. Locksley. 2008. Homeostasis and effector function of lymphopenia-induced "memory-like" T cells in constitutively T cell-depleted mice. *J. Immunol.* 180: 4742–4753.
25. Bendelac, A., P. Matzinger, R. A. Seder, W. E. Paul, and R. H. Schwartz. 1992. Activation events during thymic selection. *J. Exp. Med.* 175: 731–742.
26. Azzam, H. S., A. Grinberg, K. Lui, H. Shen, E. W. Shores, and P. E. Love. 1998. CD5 expression is developmentally regulated by T cell receptor (TCR) signals and TCR avidity. *J. Exp. Med.* 188: 2301–2311.
27. Aliahmad, P., and J. Kaye. 2008. Development of all CD4 T lineages requires nuclear factor TOX. *J. Exp. Med.* 205: 245–256.
28. Albu, D. I., D. Feng, D. Bhattacharya, N. A. Jenkins, N. G. Copeland, P. Liu, and D. Avram. 2007. BCL11B is required for positive selection and survival of double-positive thymocytes. *J. Exp. Med.* 204: 3003–3015.
29. Hettmann, T., J. DiDonato, M. Karin, and J. M. Leiden. 1999. An essential role for nuclear factor kappaB in promoting double positive thymocyte apoptosis. *J. Exp. Med.* 189: 145–158.
30. Ma, A., J. C. Pena, B. Chang, E. Margosian, L. Davidson, F. W. Alt, and C. B. Thompson. 1995. Bclx regulates the survival of double-positive thymocytes. *Proc. Natl. Acad. Sci. USA* 92: 4763–4767.
31. Teh, H. S., P. Kisielow, B. Scott, H. Kishi, Y. Uematsu, H. Blüthmann, and H. von Boehmer. 1988. Thymic major histocompatibility complex antigens and the alpha beta T-cell receptor determine the CD4/CD8 phenotype of T cells. *Nature* 335: 229–233.
32. Barnden, M. J., J. Allison, W. R. Heath, and F. R. Carbone. 1998. Defective TCR expression in transgenic mice constructed using cDNA-based alpha- and beta-chain genes under the control of heterologous regulatory elements. *Immunol. Cell Biol.* 76: 34–40.
33. Jimi, E., I. Strickland, R. E. Voll, M. Long, and S. Ghosh. 2008. Differential role of the transcription factor NF-kappaB in selection and survival of CD4+ and CD8+ thymocytes. *Immunity* 29: 523–537.
34. Matsuzawa, A., P. H. Tseng, S. Vallabhapurapu, J. L. Luo, W. Zhang, H. Wang, D. A. Vignali, E. Gallagher, and M. Karin. 2008. Essential cytoplasmic translocation of a cytokine receptor-assembled signaling complex. *Science* 321: 663–668.
35. Yamamoto, M., T. Okamoto, K. Takeda, S. Sato, H. Sanjo, S. Uematsu, T. Saitoh, N. Yamamoto, H. Sakurai, K. J. Ishii, et al. 2006. Key function for the Ubc13 E2 ubiquitin-conjugating enzyme in immune receptor signaling. *Nat. Immunol.* 7: 962–970.
36. Schmidt-Supprian, M., G. Courtois, J. Tian, A. J. Coyle, A. Israël, K. Rajewsky, and M. Pasparakis. 2003. Mature T cells depend on signaling through the IKK complex. *Immunity* 19: 377–389.
37. Skaug, B., X. Jiang, and Z. J. Chen. 2009. The role of ubiquitin in NF-kappaB regulatory pathways. *Annu. Rev. Biochem.* 78: 769–796.
38. Iwai, K., and F. Tokunaga. 2009. Linear polyubiquitination: a new regulator of NF-kappaB activation. *EMBO Rep.* 10: 706–713.
39. Xia, Z. P., L. Sun, X. Chen, G. Pineda, X. Jiang, A. Adhikari, W. Zeng, and Z. J. Chen. 2009. Direct activation of protein kinases by unanchored polyubiquitin chains. *Nature* 461: 114–119.
40. Schmidt-Supprian, M., J. Tian, H. Ji, C. Terhorst, A. K. Bhan, E. P. Grant, M. Pasparakis, S. Casola, A. J. Coyle, and K. Rajewsky. 2004. I kappa B kinase 2 deficiency in T cells leads to defects in priming, B cell help, germinal center reactions, and homeostatic expansion. *J. Immunol.* 173: 1612–1619.
41. Sato, T., S. Ohno, T. Hayashi, C. Sato, K. Kohu, M. Satake, and S. Habu. 2005. Dual functions of Runx proteins for reactivating CD8 and silencing CD4 at the commitment process into CD8 thymocytes. *Immunity* 22: 317–328.
42. Taniuchi, I., M. Osato, T. Egawa, M. J. Sunshine, S. C. Bae, T. Komori, Y. Ito, and D. R. Littman. 2002. Differential requirements for Runx proteins in CD4 repression and epigenetic silencing during T lymphocyte development. *Cell* 111: 621–633.
43. Egawa, T., and D. R. Littman. 2008. ThPOK acts late in specification of the helper T cell lineage and suppresses Runx-mediated commitment to the cytotoxic T cell lineage. *Nat. Immunol.* 9: 1131–1139.
44. Rincón, M., A. Whitmarsh, D. D. Yang, L. Weiss, B. Dérijard, P. Jayaraj, R. J. Davis, and R. A. Flavell. 1998. The JNK pathway regulates the In vivo deletion of immature CD4(+)CD8(+) thymocytes. *J. Exp. Med.* 188: 1817–1830.